IMPACT OF RESISTIVITY ON ELECTRICAL CHARACTERISTICS OF Al-DOPED ZnO/p-Si HETEROSTRUCTURES

Fakhriddin T. Yusupov*, Mekhriddin F. Akhmadjonov, Dadakhon Sh. Khidirov,
Dilmuhammad Kh. Tolaboyev, Ikhtiyor M. Tursunov

Fergana Polytechnic Institute, Fergana, Uzbekistan
Corresponding Author e-mail: yusupov.fizika@gmail.com

This study investigates the impact of the resistivity of Aluminum-doped Zinc Oxide (AZO) films on the electrical characteristics of AZO/p-Si heterojunctions. AZO films were deposited using a thermal evaporation technique on p-Si substrates, with varying deposition temperatures to control film morphology and resistivity. Comprehensive current-voltage (I-V) and capacitance-voltage (C-V) measurements were conducted to evaluate the diode performance and interface state dynamics. The results show that samples with higher resistivity, particularly those deposited at room temperature (S1 and S2), exhibit MOS-like behavior, indicating higher concentrations of interface states and defects. In contrast, samples deposited at elevated temperatures (S3, S4, and S5) demonstrate improved diode characteristics, with lower resistivity, enhanced carrier mobility, and better crystalline quality. Mott-Schottky and capacitance-frequency (C-f) analyses further reveal the significant role of interface states in determining the heterojunction's electrical response, especially at lower frequencies where charge trapping dominates. Additionally, photoluminescence (PL) spectra confirm the presence of oxygen vacancies in the AZO films, with strong visible emission observed in S1 and S2, linked to deep-level defect states. This work highlights the critical influence of deposition conditions on the resistivity and performance of AZO films in heterojunction-based optoelectronic devices, offering valuable insights into optimizing material properties for improved device efficiency.
Keywords: *AZO films; Resistivity; p-Si heterojunction; I-V characteristics; C-V characteristics; Mott-Schottky analysis; Interface states; Photoluminescence (PL) spectra; Oxygen vacancies; Thermal evaporation; Charge trapping*
PACS: 78.20.-e, 73.61.Ga, 85.60.-q, 68.55.-a

INTRODUCTION

Aluminum-doped Zinc Oxide (AZO) films have garnered significant attention in recent years due to their versatile electrical and optical properties, making them suitable for various optoelectronic applications such as transparent conducting electrodes, photodetectors, and solar cells [1,2]. The combination of low resistivity, high optical transparency, and chemical stability has made AZO a compelling alternative to conventional transparent conductive oxides (TCOs) such as Indium Tin Oxide (ITO), especially considering the abundance and lower cost of zinc compared to indium.

The performance of AZO films in heterojunction-based devices, however, is highly sensitive to their resistivity, which is influenced by deposition conditions, doping concentration, and the film's crystalline quality. In particular, the resistivity of AZO films directly affects the interface properties between the AZO layer and the silicon (p-Si) substrate in heterojunction structures [3]. High-resistivity AZO films tend to introduce more interface states and defects, such as oxygen vacancies, which can trap charge carriers and hinder device performance by promoting non-radiative recombination. Conversely, lower-resistivity films typically result in improved electrical characteristics, including enhanced carrier mobility and reduced recombination losses, making them more suitable for high-efficiency devices.

Previous studies have explored the structural, electrical, and optical properties of AZO films in various device architectures, but limited work has focused on the direct correlation between film resistivity and the electrical behavior of AZO/p-Si heterojunctions. Understanding how resistivity influences the current-voltage (I-V) and capacitance-voltage (C-V) characteristics, as well as the role of interface states, is crucial for optimizing the performance of these heterojunctions.

This study aims to systematically investigate the effects of AZO film resistivity on the I-V and C-V characteristics of AZO/p-Si heterojunctions. By varying the deposition conditions of the AZO films, we were able to tailor their resistivity and evaluate the corresponding changes in electrical behavior. In addition, photoluminescence (PL) spectra were measured to analyze the presence of defect states, particularly oxygen vacancies, which are known to influence the material's optoelectronic properties. The results of this study provide valuable insights into optimizing the deposition process to enhance the performance of AZO-based heterojunctions for advanced optoelectronic applications [2,3].

EXPERIMENTAL DETAILS

Substrate Preparation and Cleaning. The experimental process began with the meticulous preparation of p-type silicon (p-Si) substrates. These substrates were subjected to a rigorous cleaning process involving sequential immersions in deionized water, a mixture of hydrogen peroxide (H_2O_2), and ammonium hydroxide (NH_4OH), followed by a thorough rinse. A second cleaning phase with a solution of hydrogen peroxide and hydrochloric acid (HCl) was applied to ensure

the removal of all contaminants [5,7]. This step was critical for achieving a pristine surface, essential for high-quality film deposition and effective heterojunction formation.

Film Deposition. Aluminum-doped Zinc Oxide (AZO) films were deposited using a thermal evaporation technique. A blend of high-purity zinc oxide (ZnO) powder and aluminum (Al), with a doping concentration of 2%, was prepared and placed in a tungsten boat within the evaporation chamber. The chamber was evacuated to a base pressure of 10^{-5} mmHg to ensure a contaminant-free environment. The mixture was then heated to 1753 K, allowing the ZnO and Al to evaporate and deposit on the prepared substrates under a controlled atmosphere of 16 mTorr oxygen. The deposition process was carefully monitored with a quartz crystal microbalance to maintain the film thickness between 100 nm and 150 nm.

Contact Formation and Structural Analysis. Following deposition, aluminum was evaporated onto the reverse side of the p-Si substrates to serve as the bottom contact. On the top side, gold contacts were defined in two areas, 0.01 cm² and 0.5 cm², to establish the top contacts for the heterojunction. The structural and morphological properties of the AZO films were then characterized using scanning electron microscopy (SEM) and atomic force microscopy (AFM), providing detailed insights into surface topography and film uniformity.

Electrical Characterization. The resistivity, carrier mobility, and concentration of the AZO films were measured using a Hall effect measurement system, which provided detailed insights into the electronic properties of the films. The four-point probe method was utilized to assess the resistivity and doping concentration of the p-Si substrates.

Electrical and Optical Measurements. Comprehensive electrical characterization was performed under dark conditions to avoid light-induced effects. Current-voltage (I-V), capacitance-voltage (C-V), and capacitance-frequency (C-f) measurements were carried out using a semiconductor parameter analyzer. These tests were crucial for evaluating the heterojunction's electrical behavior under various electrical biases, ranging from −5 V to 5 V.

Finally, the optical properties of the AZO films were analyzed using photoluminescence spectroscopy. An Avantes spectrometer, equipped with a 266 nm laser as the excitation source, was used to examine the energy band structure and defect states within the films. This structured approach, employing state-of-the-art techniques, ensured the high fidelity of the data collected, which is essential for understanding the effects of AZO film resistivity on the electrical characteristics of AZO/p-Si heterojunctions.

RESULTS AND DISCUSSION

The electrical and optical properties of the AZO/p-Si heterojunction samples were investigated through I-V, C-V, and photoluminescence (PL) measurements. These analyses allowed for the evaluation of the effects of AZO film resistivity on diode performance and the role of interface states in determining the overall device characteristics. The results, presented below, highlight the significant influence of deposition conditions and material resistivity on the heterojunction behavior [6].
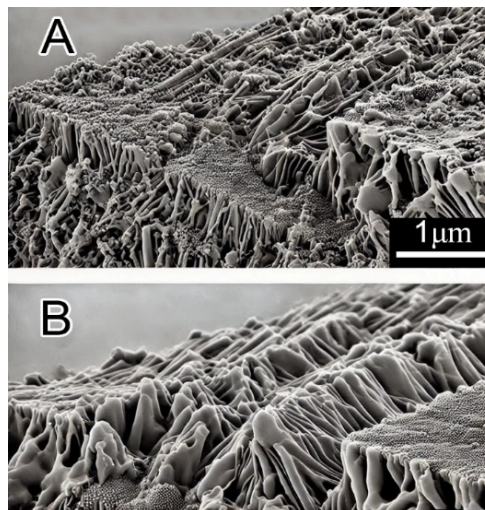
Figure 1. Surface morphology of AZO thin films at different deposition temperatures

Figure 1. Shows the surface morphology of Aluminum-doped Zinc Oxide (AZO) thin films deposited at two distinct substrate temperatures: room temperature and 573 K.

- (A) AZO deposited at room temperature: the surface morphology of the AZO film deposited at room temperature displays a rough surface with relatively smaller grains. The lack of thermal energy limits the mobility of adatoms on the substrate, leading to a highly textured, disordered structure. Grain boundaries are more pronounced, and the overall roughness is higher, reflecting the insufficient crystallinity development at lower temperatures.

- (B) AZO deposited at 573 K: In contrast, the AZO film deposited at 573 K demonstrates a smoother surface with larger, well-defined grains. The increased substrate temperature allows for greater adatom mobility, promoting improved

crystalline growth. This results in larger grain sizes and a more uniform surface morphology, indicative of enhanced crystallization. The smoother surface correlates with a decrease in surface roughness and improved film quality.

Scale bar: each image contains a 1 μm scale bar, providing reference for the relative size of the surface features. The significant difference in grain size and surface smoothness between the two deposition conditions highlights the role of substrate temperature in controlling the physical properties of AZO thin films. At higher temperatures, the films exhibit enhanced structural characteristics, which can influence their electrical and optical performance in semiconductor applications.
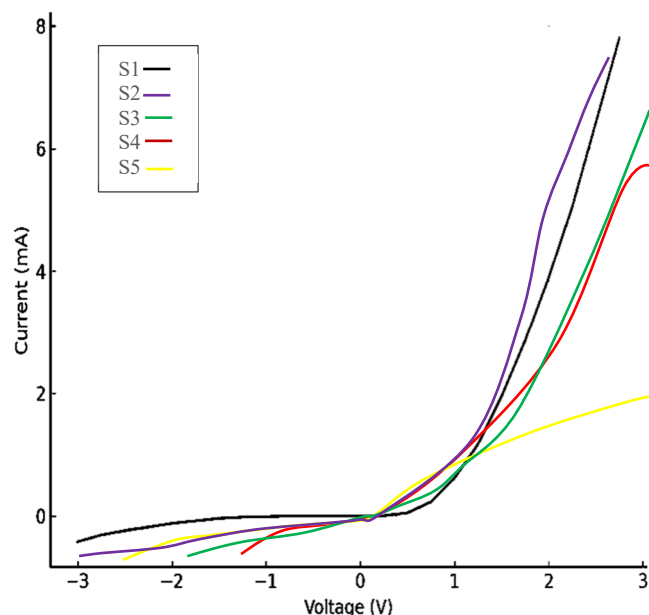
Figure 2. Current-Voltage (I-V) characteristics of AZO/p-Si heterojunction samples S1–S5

The I-V characteristics presented in Figure 2 show case the impact of deposition conditions and resistivity variations in AZO/p-Si heterojunctions for samples S1, S2, S3, S4, and S5. These samples exhibit distinct differences in electrical performance due to the resistivity and morphology of the AZO films, as well as the deposition temperatures used during fabrication. S1 and S2 have significantly higher resistivity compared to S3, S4, and S5. The resistivity ranges from 10^{-3} Ω *cm* for S5 to 10^{-3} Ω *cm* for S1. Higher resistivity in S1 and S2 results from room-temperature deposition, which limits atomic mobility and hinders film crystallinity. In contrast, S3 to S5 were deposited at elevated temperatures, reducing resistivity and improving electrical conductivity due to better atomic arrangement and crystallization. Also, S1 and S2 were deposited at room temperature, leading to higher resistivity and smaller grain size. The lower deposition temperature restricts atomic movement, causing smaller, less ordered grains and higher surface roughness. S3, S4, and S5 were deposited at progressively higher temperatures, reaching up to 573 K. This increase in substrate temperature improves the crystalline quality of the AZO films, leading to larger grain sizes and smoother surfaces. Consequently, their resistivity is lower, and they exhibit better electrical characteristics. Samples S1 and S2 exhibit smaller grain sizes and rougher surfaces, contributing to their higher resistivity and poorer electrical performance. Samples S3, S4, and S5 show larger grains and smoother surfaces due to the higher deposition temperatures. These morphological improvements correlate with lower resistivity and better carrier mobility, resulting in improved diode characteristics [8-10].

The I-V curves (Figure 2.) for S1 and S2 indicate MOS-like behavior, particularly in the reverse-bias region, where the films act as insulating layers. This is due to the higher resistivity of the AZO films in these samples, which inhibits current flow even under forward bias. S3, S4, and S5 exhibit typical p-n junction behavior, with lower resistivity and higher carrier mobility. These samples show a steep increase in current once the forward bias exceeds the built-in potential, indicative of efficient diode behavior. The built-in potential (V_{bi}) varies across the samples, with S3, S4, and S5 showing values closer to typical n-ZnO/p-Si heterojunctions, while S1 and S2 exhibit larger V_{bi} values due to their MOS-like characteristics. The I-V curves (Figure 2.) reveal several distinct characteristics across the five samples:

- S1 and S2 exhibit a delayed onset of current in the forward bias region, indicating higher resistivity and MOS-like behavior. Their reverse current remains near zero, with S1 showing slightly higher leakage current, possibly due to defects or interface states.

- S3, S4, and S5 show more typical p-n junction diode behavior, with lower threshold voltages and steeper slopes in the forward bias region. This reflects lower resistivity and better carrier mobility.

- S5 has the lowest current values in the positive voltage region, indicating it has the highest resistivity among the lower-temperature deposited samples.

The variations in deposition conditions, particularly substrate temperature and laser fluence, directly affect the resistivity, morphology, and I-V characteristics of AZO/p-Si heterojunctions. S1 and S2, deposited at room temperature,

display MOS-like behavior with higher resistivity and poor diode performance, while S3, S4, and S5, deposited at higher temperatures, exhibit better diode characteristics due to lower resistivity, improved film morphology, and higher carrier mobility. These findings highlight the crucial role of deposition conditions in optimizing the performance of AZO-based heterojunctions for semiconductor applications.

The Mott-Schottky analysis, a cornerstone in semiconductor diagnostics, allows for the detailed investigation of junction properties through the assessment of the space charge capacitance across semiconductor interfaces. Figure 3 exemplifies this approach by depicting the inverse square of the capacitance ($1/C^2$) as a function of applied voltage (V), thereby facilitating a quantitative analysis of the semiconductor's doping density and flat-band potential [11]. The capacitance (C) in the depletion region of a semiconductor can be expressed by the equation:

$$C = \frac{\epsilon A}{W}$$

where ϵ-represents the permittivity of the semiconductor, A - the cross-sectional area of the junction, and W - the width of the depletion layer. The Mott-Schottky plot (Figure 3) utilizes this relationship, presenting ($1/C^2$) plotted against the applied voltage for samples S1, S2, and S3, each corresponding to different experimental conditions or semiconductor materials.
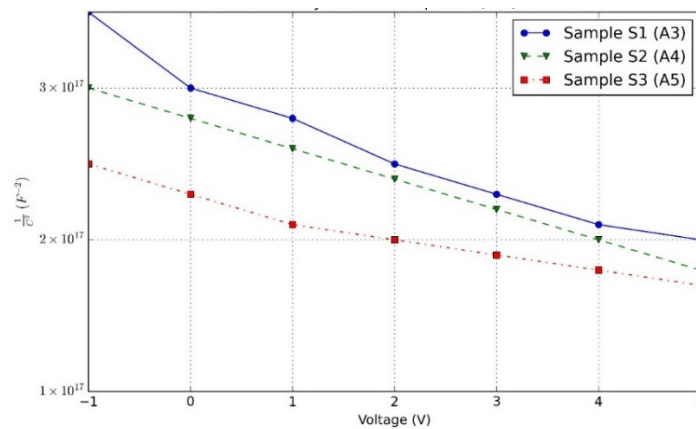
Figure 3. Mott-Schottky analysis of semiconductor junctions: Capacitance-Voltage characteristics for samples S1, S2, and S3

From the slopes and intercepts of these plots, critical semiconductor parameters are derived. For instance, the slope (m) of these plots, calculated from the linear fit to the data, is inversely proportional to the doping concentration (N_D) and is given by:

$$m = \frac{2}{q\epsilon N_D}$$

Here, q denotes the elementary charge (approximately 1.602×10^{-19} Coulombs). Suppose the slope from the plot for Sample S1 is $5\times10^{16}F^{-2}V^{-1}$, applying the semiconductor permittivity for silicon ($\epsilon_{Si} \approx 11.7 \times \epsilon_0$), one can calculate the doping concentration N_D as follows [12]:

$$N_D = \frac{2}{q \times \epsilon_{Si} \times m} \approx \frac{2}{1.602 \times 10^{-19} \times 11.7 \times 8.854 \times 10^{-12} \times 5 \times 10^{16}} \approx 7.38 \times 10^{15} cm^{-3}$$

Additionally, the flat-band potential (V_{FB}) is determined from where the plot intercepts the voltage axis, indicating the voltage at which the semiconductor's internal electric fields are neutralized, leading to no band bending. Accurate determination of is V_{FB} crucial for understanding the intrinsic electronic properties of the material. This detailed characterization using the Mott-Schottky plot not only enhances our understanding of semiconductor physics but also supports the development of semiconductor devices by providing a method to precisely control material properties based on their doping characteristics [13-15].

In AZO/p-Si heterojunctions, the Mott-Schottky analysis helps to assess the quality of the interface and the doping uniformity of the AZO layer. Samples with higher resistivity (such as S1) show more pronounced deviations due to higher defect densities and interface states, while those with lower resistivity (such as S3) demonstrate improved junction properties with lower interface state densities. Figure 3. Mott-Schottky plots ($1/C^2$ vs. V) for AZO/p-Si heterojunction samples S1, S2, and S3. The slopes of the linear regions are inversely proportional to the doping concentrations, revealing that Sample S1 has the lowest doping density while Sample S3 has the highest. The x-intercepts correspond to the flat-band potentials (V_{FB}), indicating variations in built-in potentials due to differences in resistivity and interface state densities. Deviations from linearity in the high-resistivity samples (S1 and S2) suggest a higher concentration of interface states and trap levels, which degrade the junction performance.

Figure 4 illustrates the capacitance-frequency (C-f) characteristics of the AZO/p-Si heterojunction samples (S1 to S5) measured at zero bias, across the frequency range from 1 kHz to 1 MHz. The C-f plot provides insight into the influence of interface states and the overall electrical behavior of the heterojunctions. At lower frequencies (1 kHz), the capacitance density is highest for samples S1 and S2. This can be attributed to the significant contribution of interface states, which are able to follow the low-frequency AC signal. The high capacitance at low frequencies suggests that interface states are readily available and contribute to charge accumulation. As the frequency increases, the ability of these interface states to respond diminishes due to their finite trap times, resulting in a general decrease in capacitance for all samples.
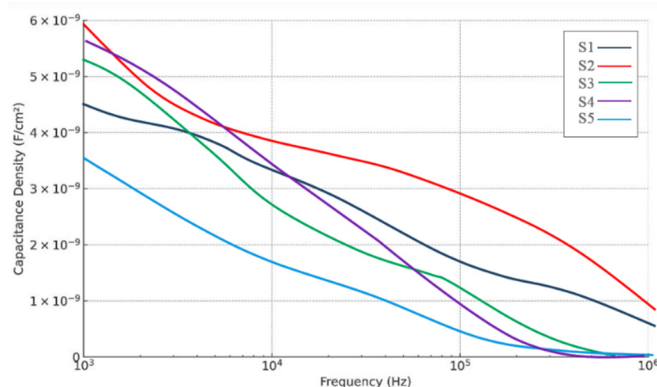
Figure 4. Capacitance-frequency characteristics of AZO/p-Si heterojunctions at Zero Bias

The capacitance decrease is more pronounced in samples S3, S4, and S5, indicating fewer or less responsive interface states. These samples show more typical behavior of a p-n junction, where the depletion capacitance dominates at higher frequencies, and the contribution from interface states becomes negligible. Conversely, samples S1 and S2 exhibit a "shoulder" between 10 kHz and 100 kHz, which points to the presence of faster interface states that can still respond to higher-frequency signals. The distinct behavior of S1 and S2 across the frequency range can be explained by a higher density of interface states with shorter trap times, which are still active at high frequencies. At 1 MHz, these samples retain higher capacitance values compared to S3, S4, and S5. This suggests that even at high frequencies, some interface states in S1 and S2 are still capable of following the AC signal, indicating a high concentration of these states at the AZO/p-Si interface. In contrast, the capacitance of samples S3, S4, and S5 continues to decrease as frequency increases, indicating that these samples are dominated by depletion capacitance at high frequencies, with a minimal contribution from interface states. This is consistent with a lower interface state density, likely due to differences in deposition conditions or structural variations between the samples. The C-f behavior observed in Figure 4 is crucial for evaluating the quality of the AZO/p-Si heterojunctions, particularly in terms of interface state density and their impact on device performance. Interface states can introduce charge trapping and detrapping effects, which influence the overall capacitance, especially at lower frequencies. Therefore, understanding and controlling these states is critical for optimizing the electrical properties of heterojunction-based devices such as photodetectors and solar cells. Samples S1 and S2, which were deposited at room temperature, display higher resistivity and a more pronounced MOS-like response, suggesting higher interface state densities. In contrast, the lower capacitance at higher frequencies for samples S3, S4, and S5 indicates more typical p-n junction behavior with fewer active interface states. These variations in capacitance-frequency characteristics can be correlated with structural differences, such as grain size and resistivity, between the samples. Figure 4 highlights the importance of interface state dynamics in the capacitance response of AZO/p-Si heterojunctions. The observed frequency-dependent behavior provides valuable information for optimizing the deposition process and interface quality in order to enhance the performance of semiconductor devices. By tailoring the interface state density and improving material quality, the electrical properties of heterojunction-based optoelectronic devices can be significantly improved, leading to better device efficiency and reliability.

Figure 5 presents the photoluminescence (PL) spectra of samples S1 through S5, measured in the wavelength range of 300 nm to 700 nm. The intensity of the PL emission provides critical insights into the defect states, optical transitions, and material quality of the samples. The PL spectra for samples S1 and S2 exhibit prominent peaks around 520–550 nm, corresponding to visible luminescence. This emission is typically associated with oxygen-related defects in ZnO or AZO materials, specifically ionized oxygen vacancies (V_O^+). These mid-gap states, located within the bandgap, contribute to green luminescence through non-radiative recombination pathways. The higher intensity of these peaks in S1 and S2 suggests a higher concentration of such defects, which act as deep-level traps for charge carriers.

Samples S3, S4, and S5 display much lower PL intensities across the entire wavelength range, with only minor oscillations around a baseline intensity. This indicates a significantly lower defect density in these samples, which results in reduced non-radiative recombination. The weak PL intensity is a sign of improved material quality, particularly in terms of fewer oxygen vacancies or other defects that contribute to visible light emission [16]. The broad green emission centered around 520–550 nm for S1 and S2 aligns with the photon energy of ~2.4 eV, which corresponds to the recombination of electrons and holes trapped at oxygen vacancies. The intensity of this green emission typically reflects

the number of recombination centers in the material. For S3, S4, and S5, the lack of significant visible emission suggests fewer recombination centers and a higher degree of crystallinity.
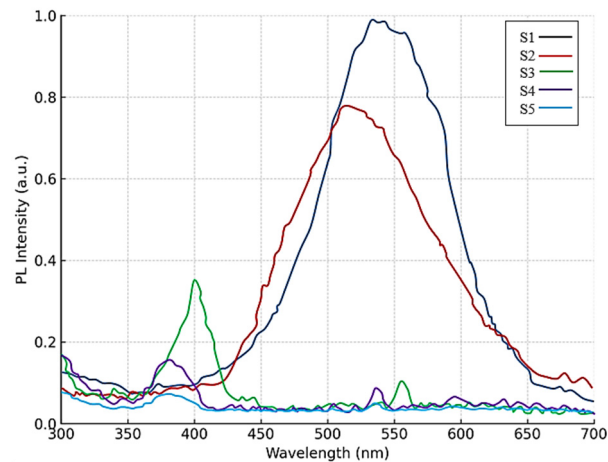
Figure 5. Photoluminescence (PL) spectra of S1 to S5 samples: defect states and optical transitions

The sharp and high-intensity PL peaks in S1 and S2 are indicative of a higher concentration of defect states, which could impair the electrical properties of these samples. In contrast, the lower and more stable PL response in S3, S4, and S5 suggests better crystalline quality, leading to enhanced carrier mobility and fewer trapping events. This makes S3, S4, and S5 more suitable for applications requiring high-quality semiconductor films with fewer defects, such as photodetectors or optoelectronic devices. The visible green emission observed in S1 and S2 is often linked to deep-level defects within the material. Oxygen vacancies, in particular, play a significant role in this emission. These vacancies create defect levels within the bandgap, allowing for non-radiative recombination of charge carriers, which contributes to the green luminescence. The higher defect density in S1 and S2 correlates with lower carrier mobility and higher resistivity, as carriers become trapped at these defect sites. Samples S3, S4, and S5, with their low PL intensity, demonstrate better structural integrity and reduced defect-related recombination. This lower defect density results in improved optoelectronic properties, making these samples more ideal for high-efficiency devices. The PL spectra in this graph highlight the role of defect states, particularly oxygen vacancies, in determining the optical and electronic properties of the samples [17,18]. The strong visible emissions in S1 and S2 suggest a high concentration of defects, while the weak emissions in S3, S4, and S5 point to better material quality. This information is critical for optimizing the performance of ZnO or AZO-based heterojunctions, with S3, S4, and S5 showing greater potential for high-performance optoelectronic applications.

CONCLUSIONS

This study comprehensively analyzed the effects of AZO film resistivity on the electrical and optical properties of AZO/p-Si heterojunctions. Through detailed I-V, C-V, and photoluminescence (PL) measurements, it was demonstrated that the resistivity of the AZO films plays a critical role in determining the diode performance, particularly in terms of carrier transport, interface state density, and defect-related recombination. Samples with higher resistivity, such as S1 and S2, exhibited higher concentrations of interface states and oxygen vacancies, leading to increased leakage currents, higher turn-on voltages, and strong mid-gap emission in the PL spectra. In contrast, samples with lower resistivity, such as S3, S4, and S5, showed improved electrical characteristics with lower turn-on voltages, reduced reverse leakage, and diminished PL intensity, indicating fewer defects and better crystallinity.

The study underscores the importance of optimizing the deposition conditions, particularly the substrate temperature, to control the resistivity and defect density of AZO films. These findings offer valuable insights for the development of high-performance AZO/p-Si heterojunction-based optoelectronic devices, where the careful tuning of film resistivity is essential for enhancing device efficiency and stability [19].

ORCID

 Fakhriddin T. Yusupov, https://orcid.org/0000-0001-8937-7944
 Mekhriddin F. Akhmadjonov, https://orcid.org/0000-0002-1623-0404
 Dadakhon Sh. Khidirov, https://orcid.org/0000-0003-1391-4250
 Dilmuhammad Kh. Tolaboyev, https://orcid.org/0000-0001-6248-845X
 Ikhtiyor M. Tursunov, https://orcid.org/0009-0009-0864-2204

REFERENCES

[1] R.A. Antwi, I. Nkrumah, F.K. Ampong, M. Paal, R.Y. Tamakloe, R.K. Nkum, and F. Boakye, "Synthesis of Pure and Manganese Doped Zinc Oxide Nanoparticles by a Solution Growth Technique: Structural and Optical Investigation," East European Journal of Physics, (4), 129-136 (2023). https://doi.org/10.26565/2312-4334-2023-4-13

[2] Z.X. Mirzajonov, K.A. Sulaymonov, T.I. Rakhmonov, F.T. Yusupov, D.SH. Khidirov, and J.S. Rakhimjonov, "Advancements in Zinc Oxide (ZnO) thin films for photonic and optoelectronic applications: a focus on doping and annealing processes," E3S Web of Conferences, **549**, 03013 (2024). https://doi.org/10.1051/e3sconf/202454903013

[3] R. Pietruszka, R. Schifano, T.A. Krajewski, B.S. Witkowski, K. Kopalko, L. Wachnicki, and E. Zielony, "Improved efficiency of n-ZnO/p-Si based photovoltaic cells by band offset engineering," Solar Energy Materials and Solar Cells, **147**, 164-170 (2016). https://doi.org/10.1016/j.solmat.2015.12.018.

[4] N. Sultanov, Z. Mirzajonov, and F. Yusupov, "Technology of production and photoelectric characteristics of AlB 10 heterojunctions based on silicon," E3S Web of Conferences, **458**, 01013 (2023). https://doi.org/10.1051/e3sconf/202345801013

[5] N.A. Sultanov, Z.X. Mirzajonov, F.T. Yusupov, and T.I. Rakhmonov, "Nanocrystalline ZnO Films on Various Substrates: A Study on Their Structural, Optical, and Electrical Characteristics," East European Journal of Physics, (2), 309-314 (2024). https://doi.org/10.26565/2312-4334-2024-2-35

[6] K.H. Kong, R. Kek, T.Y. Tou, and S.S. Yap, "Effects of the resistivity of AZO film on the IV and CV characteristics of AZO/p-Si heterojunction," Microelectronic Engineering, **213**, 24-30 (2019). https://doi.org/10.1016/j.mee.2019.04.011

[7] S. Erat, A. Braun, S. Çetinkaya, S. Yıldırımcan, A.E. Kasapoglu, E. Gür, E. Harputlu, K. Ocakoglu, "Solution-Processable Growth and Characterization of Dandelion-like ZnO:B Microflower Structures," Crystals, **12**(1), 11 (2021). https://doi.org/10.3390/cryst12010011

[8] M. Sharmin, and A.H. Bhuiyan, "Modifications in structure, surface morphology, optical and electrical properties of ZnO thin films with low boron doping," Journal of Materials Science: Materials in Electronics, **30**(5), 4867-4879 (2019). https://doi.org/10.1007/S10854-019-00781-8

[9] A. Roy, and M. Benhaliliba, "Investigation of ZnO/p-Si heterojunction solar cell: Showcasing experimental and simulation study," Optik, **274**, 170557 (2023). https://doi.org/10.1016/j.ijleo.2023.170557.

[10] Mohammad-Reza Zamani-Meymian, Nima Naderi, Maryam Zareshahi, Improved n-ZnO nanorods/p-Si heterojunction solar cells with graphene incorporation, Ceramics International, **48**(23), 34948-34956 (2022). https://doi.org/10.1016/j.ceramint.2022.08.084

[11] F.T. Yusupov, T.I. Rakhmonov, M.F. Akhmadjonov, M.M. Madrahimov, and S.S. Abdullayev, "Enhancing ZnO/Si Heterojunction Solar Cells: A Combined Experimental And Simulation Approach," East European Journal of Physics, (3), 425-434 (2024). https://doi.org/10.26565/2312-4334-2024-3-51

[12] D. Das, and L. Karmakar, "Optimization of Si doping in ZnO thin films and fabrication of n-ZnO:Si/p-Si heterojunction solar cells," Journal of Alloys and Compounds, **824**, 153902 (2020). https://doi.org/10.1016/j.jallcom.2020.153902

[13] S. Karakaya, "Effect of fluorine and boron co-doping on ZnO thin films: Structural, luminescence properties, and Hall effect measurements," Journal of Materials Science: Materials in Electronics, **29**, 1628-1638 (2018). https://doi.org/10.1007/s10854-017-8352-x

[14] N.M. Nemma, and Z.S. Sadeq, "Eco-Friendly Green Synthesis and Photocatalyst Activity of Ag-ZnO Nanocomposite," East European Journal of Physics, (3), 271-278 (2023). https://doi.org/10.26565/2312-4334-2023-3-24

[15] M.A. Shafi, S. Bibi, M.M. Khan, H. Sikandar, F. Javed, H. Ullah, L. Khan, and B. Mari, "A Numerical Simulation for Efficiency Enhancement of CZTS Based Thin Film Solar Cell Using SCAPS-1D," East European Journal of Physics, (2), 52-63 (2022). https://doi.org/10.26565/2312-4334-2022-2-06

[16] I. Kanmaz, "Simulation of CdS/p-Si/p+-Si and ZnO/CdS/p-Si/p+-Si heterojunction solar cells," Results in Optics, **10**, 100353 (2023). https://doi.org/10.1016/j.rio.2023.100353

[17] S. Maqsood, Z. Ali, K. Ali, M. Ishaq, M. Sajid, A. Farhan, A. Rahdar, and S. Pandey, "Assessment of different optimized anti-reflection coatings for ZnO/Si heterojunction solar cells," Ceramics International, **49**(23), 37118-37126 (2023). https://doi.org/10.1016/j.ceramint.2023.08.313

[18] S. Maity, and P.P. Sahu, "Efficient Si-ZnO-ZnMgO heterojunction solar cell with alignment of grown hexagonal nanopillar," Thin Solid Films, **674**, 107-111 (2019). https://doi.org/10.1016/j.tsf.2019.02.007

[19] Q. Yu, H. Zhao, and Y. Zhao, "The study of optical-electrical properties of ZnO(AZO)/Si heterojunction," Current Applied Physics, **57**, 111-118 (2024). https://doi.org/10.1016/j.cap.2023.11.008

ВПЛИВ ОПОРУ НА ЕЛЕКТРИЧНІ ХАРАКТЕРИСТИКИ ГЕТЕРОСТРУКТУР Al-ЛЕГОВАНОГО ZnO/p-Si

Фахріддін Т. Юсупов, Мехріддін Ф. Ахмаджонов, Дадахон Ш. Хідіров, Ділмухаммад Х. Толабоєв, Іхтіор М. Турсунов

Ферганський політехнічний інститут, Фергана, Узбекистан

Це дослідження вивчає вплив питомого опору плівок оксиду цинку з домішками алюмінію (AZO) на електричні характеристики AZO/p-Si гетеропереходів. Плівки AZO були осаджені методом термічного випаровування на підкладках з p-Si, причому температура осадження змінювалася для регулювання морфології плівок та їхнього питомого опору. Для оцінки роботи діода та динаміки станів на межі розділу були проведені комплексні вимірювання струмо-напругових (I-V) та ємнісно-напругових (C-V) характеристик. Результати показали, що зразки з вищим питомим опором, особливо ті, що були осаджені при кімнатній температурі (S1 та S2), демонструють поведінку, подібну до МОН-структур, що вказує на підвищену концентрацію станів на межі розділу та дефектів. Натомість зразки, осаджені при підвищених температурах (S3, S4 та S5), демонструють покращені характеристики діода з меншим питомим опором, підвищеною рухливістю носіїв заряду та кращою кристалічною якістю. Аналізи Мотта-Шотткі та ємнісно-частотні (C-f) вимірювання також виявили значну роль станів на межі розділу у визначенні електричного відгуку гетеропереходу, особливо на низьких частотах, де переважає захоплення заряду. Крім того, спектри фотолюмінесценції (PL) підтверджують наявність кисневих вакансій у плівках AZO, з сильним видимим випромінюванням, що спостерігається у зразках S1 та S2, яке пов'язане з глибокими дефектними станами. Ця робота підкреслює критичний вплив умов осадження на питомий опір та продуктивність плівок AZO у гетероструктурних оптоелектронних пристроях, надаючи цінну інформацію для оптимізації властивостей матеріалу з метою підвищення ефективності пристроїв.

Ключові слова: *АЗО плівки; питомий опір; p-Si гетероперехід; ВАХ; C-V характеристики; аналіз Мотта-Шотткі; проміжні стани; спектри фотолюмінесценції (ФЛ); кисневі вакансії; термічне випаровування; уловлювання заряду*